

Article

Effect of Equal Channel Angular Pressing on Microstructure and Mechanical Properties of a Cu-Mg Alloy

Muzhi Ma ¹, Xi Zhang ¹, Zhou Li ^{1,2}, Zhu Xiao ^{1,3,*}, Hongyun Jiang ⁴, Ziqi Xia ¹ and Hanyan Huang ¹

¹ School of Materials Science and Engineering, Central South University, Changsha 410083, China; mamuzhimse@163.com (M.M.); zhang_xi@csu.edu.cn (X.Z.); lizhou6931@163.com (Z.L.); xiazizhi@csu.edu.cn (Z.X.); huanghanyan@csu.edu.cn (H.H.)

² State Key Laboratory of Powder Metallurgy, Central South University, Changsha 410083, China

³ Key Laboratory of Non-Ferrous Metal Materials Science and Engineering, Ministry of Education, Changsha 410083, China

⁴ Zhejiang Tianning Alloy Material Co., Ltd., Jinhua 321002, China; jianghongyun@zjtnhj.com

* Correspondence: xiaozhumse@163.com

Received: 26 April 2020; Accepted: 26 May 2020; Published: 27 May 2020

Abstract: A Cu-0.43Mg (wt.%) alloy was processed by equal channel angular pressing (ECAP) up to eight passes via a processing route (Bc). The hardness distribution on the longitudinal and transverse sections was collected and the microstructure in the central and bottom regions on the longitudinal section was examined. The result showed that the hardness was improved significantly at the initial stage of the ECAP process, and the lower hardness region appeared at the area nearby the bottom surface. With the number of ECAP passes, the hardness gently increased and finally became saturated. The inhomogeneity of the hardness distribution along the normal direction gradually weakened and finally disappeared. The shear microstructure in the central region was different from that in the bottom region after one ECAP pass, and they became similar to each other after two ECAP passes, except the rotation angle of the elongated grains. With the further increasing ECAP passes, there was no obvious microstructure difference between the central and bottom regions. The inhomogeneities of the hardness and the microstructure along the normal direction in the alloy after one ECAP passes should be attributed to the non-zero outer arc of curvature of the ECAP die and the friction between the bottom surface of the billets and the ECAP die walls. The yield strength of the alloy increased from 124 MPa before the ECAP process to 555 MPa after eight ECAP passes. The improvement of yield strengths of the ECAPed Cu-Mg alloy should be mainly attributed to the dislocation strengthening and the grain boundary strengthening.

Keywords: Cu-Mg alloy; equal channel angular pressing (ECAP); microstructure; mechanical properties

1. Introduction

Copper alloys play a vital role in mechanical manufacturing, railway transportation, electrical and electronic industries [1–4]. Cu-Mg alloys have been widely applied as the contact wire and other conductor materials in the high-speed rail industry due to their good combination of high strength and high electrical conductivity [5–8]. However, the present Cu-Mg alloy contact wire is currently unable to meet the new requirements of higher speed, heavier haul and lower power loss of high-speed railway vehicles [9]. Many researchers have attempted to improve the comprehensive properties of the Cu-Mg alloy via the microalloying method [10–13], but the solute atoms introduced

by the microalloying method could significantly and inevitably decrease the electrical conductivity of the Cu-Mg alloy [14].

The severe plastic deformation (SPD) technique can effectively improve the strength of copper alloy without decreasing its high electrical conductivity [15]. The most attractive one is the equal channel angular pressing (ECAP) technique. It is an attractive SPD method to produce copper alloy with an ultra-fine grain (UFG). The ECAP process involves that the metallic material is deformed by pressing through an equal cross-sectional channel with the right or obtuse angle [16]. After multiple ECAP processes, the micro- or nano-scaled UFGed microstructure can be obtained, leading to the high strength of alloys according to the Hall–Petch relationship [17–20]. The dislocations and grain boundaries introduced by the ECAP process have a limited influence on the electron scattering, and thus the good electrical conductivity of the alloy can be maintained [14]. The ECAP process combined with the continuous forming (CONFORM) process can be easily incorporated to produce Cu-Mg alloy contact wire with a standard length of more than 1400 m [21]. However, the ECAP process often results in an inhomogeneous shear strain in the material [22], and leads to the different microstructure and properties in different regions of the ECAPed material [23,24]. Taking pure Al as an example, after one ECAP pass, the hardness in the region adjacent to the bottom surface (30–35 HV) was much lower than those in the other regions (40–50 HV) [23,24]. This inhomogeneity phenomenon is undoubtedly harmful to the comprehensive properties of ECAPed materials, and the microstructure evolution and its effect on the mechanical properties of the highly conductive copper alloys are worth investigating.

In this study, the effect of ECAP on the microstructure and mechanical properties of a Cu-0.43Mg (wt.%) alloy was investigated in detail. The hardness on the longitudinal and transverse sections was measured and analyzed. The microstructure in the central and bottom regions on the longitudinal section was observed by the electron back-scattered diffraction (EBSD) technique. The mechanism of the inhomogeneity phenomenon in the alloy during the ECAP process was discussed. The strengthening mechanisms of the ECAPed Cu-Mg alloy were also analyzed quantitatively.

2. Materials and Methods

The Cu-0.43Mg (wt.%) alloy was melted with the raw materials of pure copper and pure magnesium using a medium frequency induction furnace, and its chemical composition was measured using a SPECTROBLUE inductively coupled plasma optical emission spectrometer (ICP-OES) (SPECTRO Analytical Instruments GmbH, Kleve, Düsseldorf, Nordrhein-Westfalen, Germany). The ingot was homogenization treated at 780 °C for 1 h, and then hot-rolled from 35 to 12 mm in thickness, followed by water quenching. The cylindrical billets for the ECAP test were cut from the hot-rolled plate with a dimension of $\Phi 10 \times \sim 70$ mm. The ECAP process was performed at room temperature, on a 150T four-column hydraulic press, with the plug speed of ~ 10 mm/s. Figure 1a shows the schematic illustration of the ECAP process. The ECAP die was a two-piece split die, with the inner channel angle (Φ) of 110° and the outer arc of curvature (Ψ) of 30°. A suspension containing graphite and machine oil was used as the lubricant to reduce the friction between the billets and the ECAP die wall. The billets were repetitively ECAP-processed up to 8 passes via a processing route (Bc), where the billet was rotated by 90° about the longitudinal axis in the same direction between each consecutive pass [16]. The laboratory coordinate system of the ECAP process was defined as follows: X, Y and Z axes were parallel to the extrusion direction (ED), normal direction (ND) and transverse direction (TD), respectively [25].

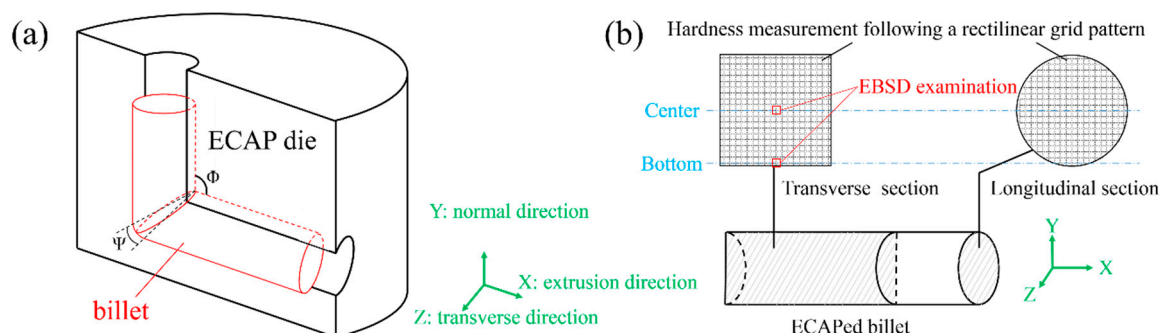


Figure 1. Schematic illustrations of (a) the equal channel angular pressing (ECAP) process and (b) the hardness measurement and electron back-scattered diffraction (EBSD) examination.

Figure 1b shows the schematic illustration of the hardness measurement and EBSD examination. Vickers hardness on the longitudinal and transverse sections of the ECAPed billets was measured following a rectilinear grid pattern with a spacing of 0.5 mm using a HV-5 microhardness tester, with a load of 1 kg and a dwell time of 15 s. The hardness was visualized in the form of a color-coded contour map in order to intuitively show the hardness distribution. The microstructure in the central and bottom regions on the longitudinal section was examined by the EBSD technique using an FEI Helios Nanolab 600i scanning electron microscope (SEM) equipped with a NordlysMax2 EBSD detector operating at an accelerating voltage of 20 keV and an electric current of 1 nA. In this case, the copper specimen had a lateral resolution of ~ 40 nm and a longitudinal resolution of ~ 100 nm. The EBSD data were analyzed using the HKL Channel5 software. The average grain size was characterized using boundaries with the misorientation angles larger than 15° and allowing completion down to 10° , and the grain areas were converted to the equivalent diameters. For the mean boundary spacing, the boundary was detected according to the critical misorientation angle of 2° , and then the mean boundary spacing was measured using the line intercept method. In addition, the boundaries with the misorientation angles larger than 15° were defined as the high-angle boundaries (HABs), and the boundaries with the misorientation angles lower than 15° but larger than 2° were defined as the low-angle boundaries (LABs).

3. Results

Figure 2 shows the color-coded contour maps of the hardness on the longitudinal section of the hot-rolled and ECAPed Cu-Mg alloy. The hardness of the hot-rolled Cu-Mg alloy was very low (75 ± 1 HV) but the distribution of hardness was homogeneous (Figure 2a). After one ECAP pass, the hardness nearly doubled to $\sim 140 \pm 3$ HV (Figure 2b). However, the hardness adjacent to the bottom surface (121 ± 4 HV) was obviously lower than that in the other regions (141 ± 2 HV), indicating an inhomogeneous hardness distribution along the Y direction. After two ECAP passes, the hardness increased to $\sim 155 \pm 3$ HV, except the low-hardness region adjacent to the bottom surface (145 ± 3 HV) (Figure 2c). In addition, the degree of hardness inhomogeneity weakened compared with that after one ECAP pass. After four, six and eight ECAP passes, the hardness gently increased to 168 ± 3 HV, 177 ± 2 HV and 181 ± 2 HV, respectively, and the hardness inhomogeneity along the Y direction disappeared (Figure 2d,f). Figure 3 shows the color-coded contour maps of the hardness on the transverse section of the hot-rolled and ECAPed Cu-Mg alloy. The result was similar to that on the longitudinal section. On the one hand, the hardness was improved significantly from 75 ± 1 HV before the ECAP process to $\sim 140 \pm 3$ HV at the initial stage of the ECAP process. Then, it gently increased to $\sim 155 \pm 3$ HV after two ECAP passes, 167 ± 3 HV after four ECAP passes, 177 ± 2 HV after six ECAP passes and finally achieved stability at 181 ± 2 HV after eight ECAP passes. On the other hand, the lower-hardness regions with the values of 121 ± 2 HV and 144 ± 3 HV occurred at the area near the bottom surface after one and two ECAP passes, respectively. Then, the degree of hardness inhomogeneity along the Y direction gradually weakened and finally disappeared.

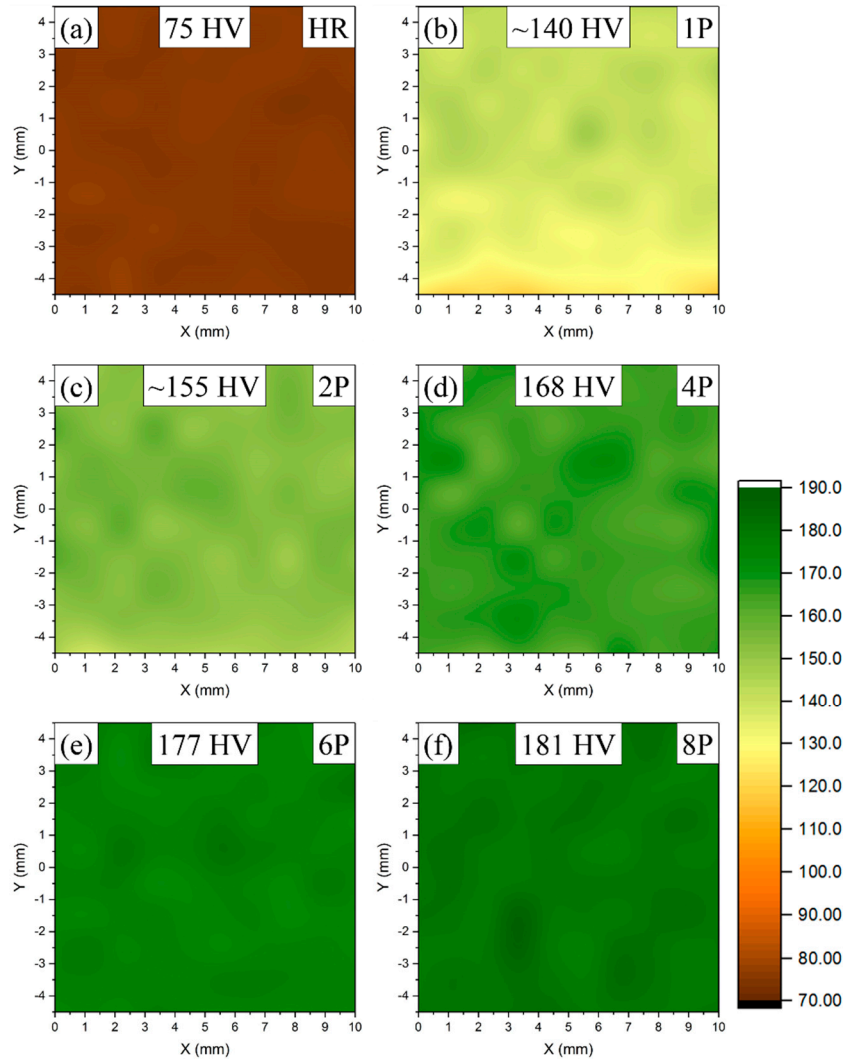


Figure 2. Color-coded contour maps of the hardness on the longitudinal section of the Cu-Mg alloy (a) before the ECAP process and after (b) 1, (c) 2, (d) 4, (e) 6 and (f) 8 ECAP passes.

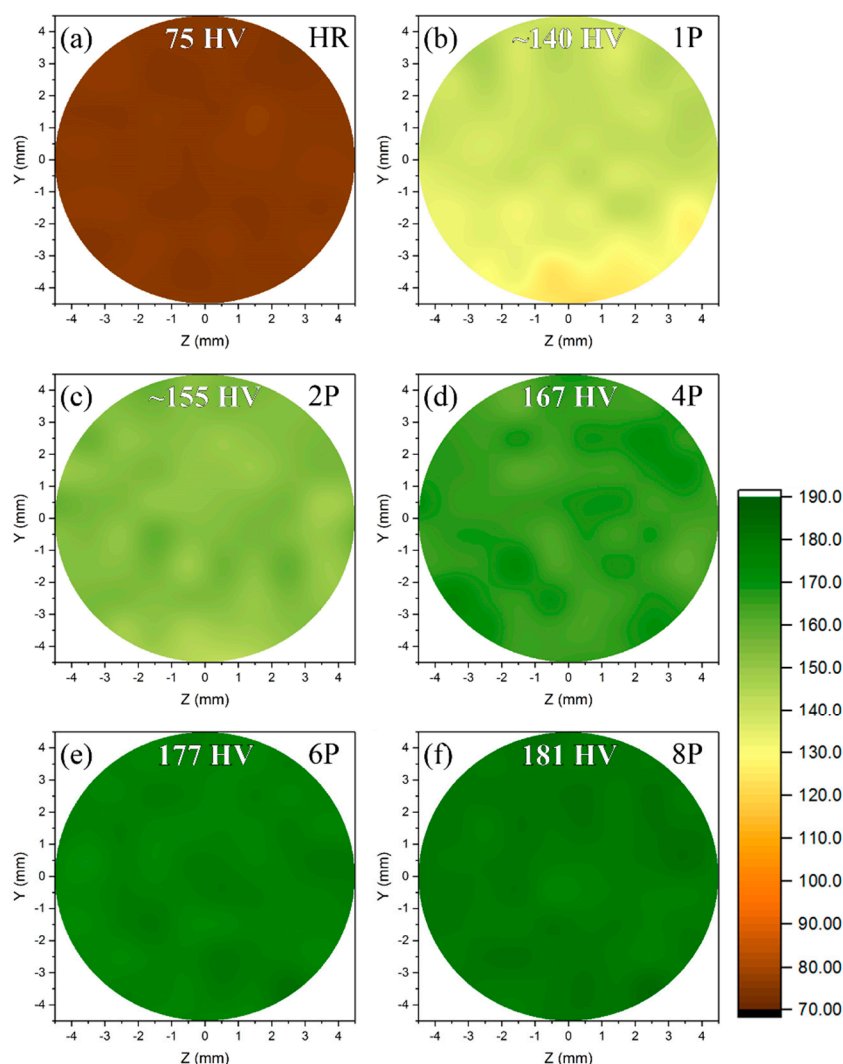


Figure 3. Color-coded contour maps of the hardness on the transverse section of the Cu-Mg alloy (a) before the ECAP process and after (b) 1, (c) 2, (d) 4, (e) 6 and (f) 8 ECAP passes.

Figures 4 and 5 show the inverse pole figure (IPF) coloring maps in the central and bottom regions on the longitudinal section of the ECAPed Cu-Mg alloy, respectively. The direction label of the ECAP process and the coloring triangle of the cupreous crystallographic orientation are shown on the lower-right regions of Figures 4 and 5. After one ECAP pass, the central region showed the shear microstructure, where the grains were elongated along the direction counter-clockwise-rotated $\sim 45^\circ$ with the ED (Figure 4a). The drastic color change inside the elongated grains indicated that a number of LABs subdivided the original hot-rolled grains. However, the bottom region showed a different microstructure consisting of the distorted equiaxed grains and twins (Figure 5a). The grain morphology was similar to that before the ECAP process, even though some dislocations appeared inside the grains. After two ECAP passes, the microstructures in the central and bottom regions were both composed of the elongated grains, but the rotation angle of the elongated grains in the central region ($\sim 45^\circ$) was higher than that in the bottom region ($\sim 20\text{--}30^\circ$) (Figures 4b and 5b). After four and six ECAP passes, the majority of the elongated grains in the central and bottom regions was refined and the grain sizes showed bimodal distributions (Figures 4c, 5c, 4d and 5d). After eight ECAP passes, the refined grains were surrounded by the HABs, indicating that the two regions achieved the UFGed microstructure (Figures 4e and 5e).

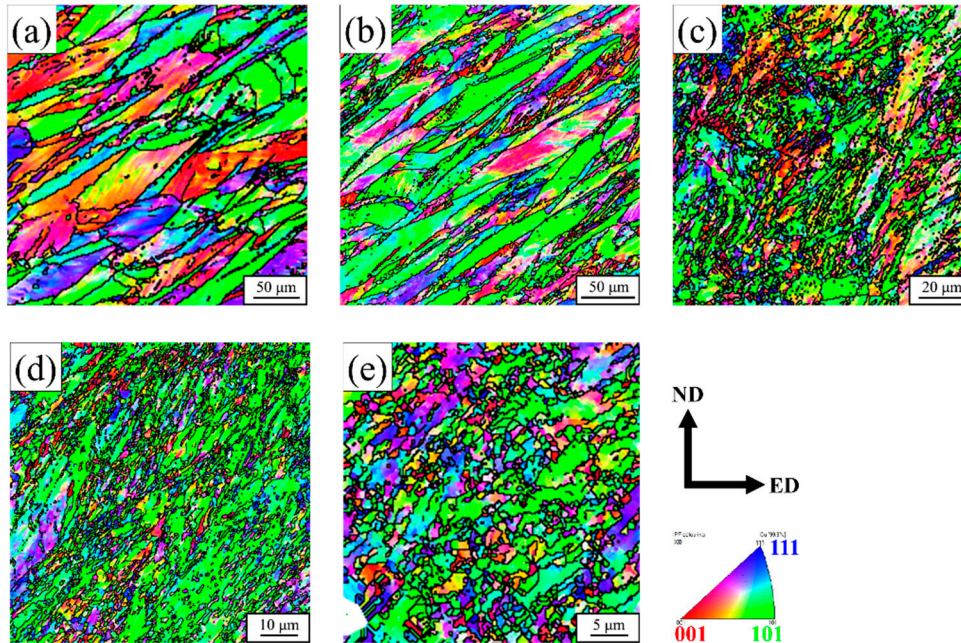


Figure 4. Inverse pole figure (IPF) coloring maps in the central region on the longitudinal section of the ECAPed Cu-Mg alloy: (a) 1, (b) 2, (c) 4, (d) 6 and (e) 8 ECAP passes.

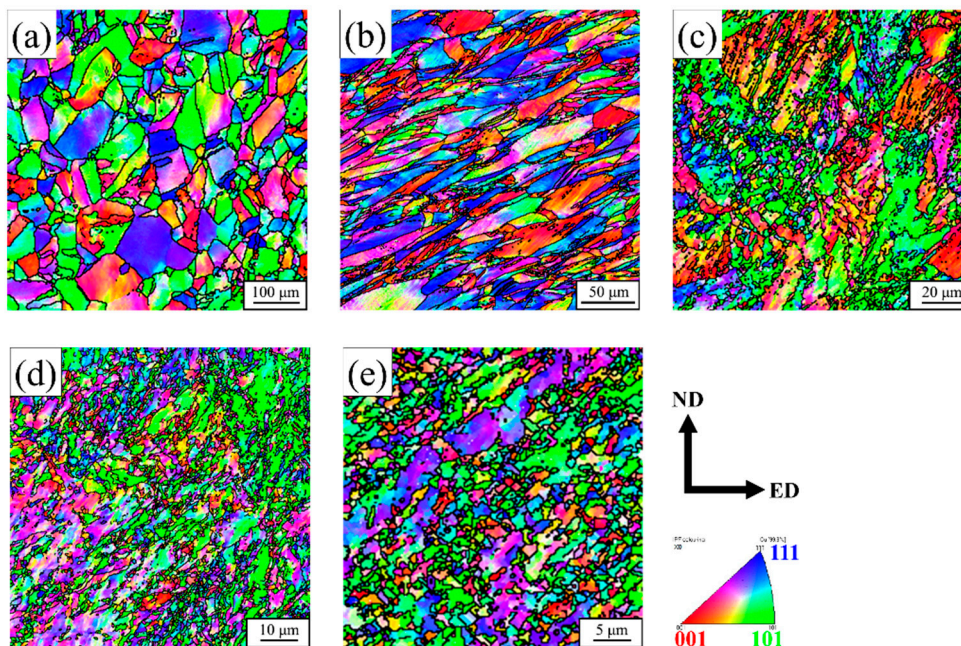


Figure 5. IPF coloring maps in the bottom region on the longitudinal section of the ECAPed Cu-Mg alloy: (a) 1, (b) 2, (c) 4, (d) 6 and (e) 8 ECAP passes.

Figure 6 shows the microstructure information in the central and bottom regions on the longitudinal section of the ECAPed Cu-Mg alloy. The average grain size and the mean boundary spacing decreased with the number of ECAP passes (Figure 6a,b). After the first four ECAP passes, the average grain size decreased rapidly from dozens of micrometers before the ECAP process [15] to two or three micrometers, and the mean boundary spacing also decreased sharply from several hundred micrometers before the ECAP process [15] to less than one micrometer. In the subsequent ECAP process, the average grain size and the mean boundary spacing gradually reached saturation.

In addition, it should be noted that at the initial stage of the ECAP process, the two parameters in the central region were lower than those in the bottom region, but this difference disappeared after the fourth ECAP pass. For the other two parameters, at the initial stage of the ECAP process, the dislocations and the subgrain boundaries were predominant, and thus the fraction of HABs and the mean misorientation angle of LABs showed the low values (Figure 6c,d). With of the increasing ECAP passes, the subgrain boundaries absorbed dislocations to increase its misorientation angle and transform into HABs, leading to the increase in the fraction of HABs and the mean misorientation angle of LABs.

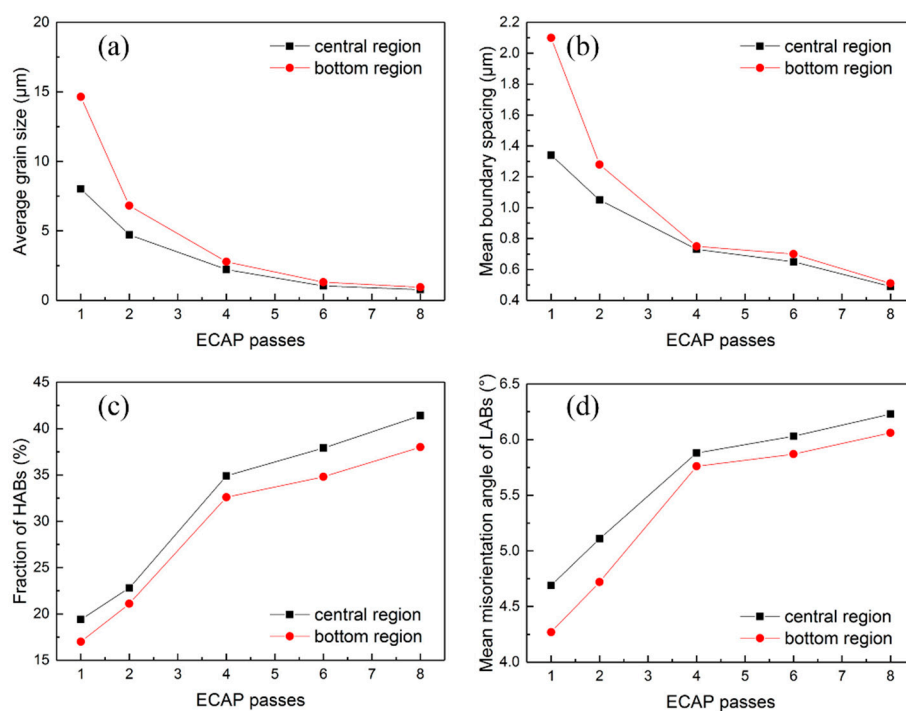


Figure 6. Microstructure information in the central and bottom regions on the longitudinal section of the ECAPed Cu-Mg alloy: (a) average grain size, (b) mean boundary spacing, (c) fraction of high-angle boundaries (HABs) and (d) mean misorientation angle of low-angle boundaries (LABs).

4. Discussion

4.1. Mechanism for Inhomogeneity Phenomenon

It is noted that the hardness and microstructure of the Cu-Mg alloy after one ECAP pass are very inhomogeneous along the Y direction, however, this inhomogeneity phenomenon gradually weakens and finally disappears with the number of ECAP passes. This is consistent with some previous research works on pure Al and Al alloys [26–28]. The inhomogeneity phenomenon at the initial stage of the ECAP process could be attributed to the formation of a corner gap [26–28]. At the corner gap, the billets no longer contact with the ECAP die walls and in turn the die walls no longer impose the shear strain on the billets. Thus, the inhomogeneous strain imposed on the billets results in the uneven distribution of the hardness and microstructure. However, the formation of a corner gap is related to the outer arc of curvature of the ECAP die. It was reported that a smaller corner gap was found when using an ECAP die with a high outer arc of curvature [29]. Therefore, the reason for the inhomogeneity phenomenon should be reconsidered.

An ideal ECAP process is considered as a simple shear deformation, with the shear direction from the inner corner to the outer corner of channel and the shear plane located on the intersection plane of the two parts of the channel [22]. However, the inevitable shear stress derived from the friction between the bottom surface of the billets and the ECAP die walls is often ignored [30–32]. Thus, the practical ECAP process becomes a complicated deformation combining the ideal simple

shear deformation and the frictional shear deformation near the bottom surface. In addition, the non-zero outer arc of curvature expands the main plastic deformation zone (MPDZ) of the ideal ECAP process from the intersection plane of the two parts of the channel into the fan-shaped zone, which is sharp at the inner corner and broadens towards the outer corner [33,34]. When the billets pass through the MPDZ, the distribution of the equivalent strain rate ($\dot{\epsilon}$) along the Y direction becomes inhomogeneous [35]. The more adjacent to the bottom surface the region is, the lower the equivalent strain rate is. For a special situation of $\dot{\epsilon} = 0$, it means that only rigid-body rotation occurs in the grains, rather than plastic deformation.

These additional factors have a great influence on the microstructure and mechanical properties of the ECAPed Cu-Mg alloy. Firstly, in the initial stage of the ECAP process, the region adjacent to the bottom surface goes through such little plastic deformation that only a small number of dislocations need be activated to accommodate it. When the billet is pressed through the ECAP die, only the kinematical rigid-body rotation occurs in the alloy [36]. Thus, the grain morphology could not obviously change compared with the hot-rolled one, except a slight distortion of grains, and the hardness is also lower than those in other regions. Secondly, the region adjacent to the bottom surface shows the lower rotation angle of the elongated grains due to the additional frictional shear stress parallel to the ED. The EBSD result confirmed that the rotation angle of the elongated grains in the bottom region after two ECAP passes is 20°–30° but that in the central region, it is ~45°. Thirdly, the grain refinement during the ECAP process is based on the dislocation subdivision mechanism [37]. The accumulation rate of dislocations determines the rate of microstructure evolution. Therefore, in the bottom region, the average grain size and the mean boundary spacing are higher, and the fraction of HABs and the mean misorientation angle of LABs are lower. In addition, it should be noted that the route Bc also plays an important role in the weakening and disappearance of inhomogeneity. The bottom region after the first ECAP pass is not the bottom region after the second ECAP pass.

4.2. Strengthening Mechanisms and Strengths Calculation

The strengthening mechanisms of the ECAPed Cu-Mg alloy can be considered from four aspects and its yield strength can be expressed as Equation (1) [38]:

$$\sigma_y = \sigma_{LF} + \sigma_{SS} + \sigma_D + \sigma_{GB} \quad (1)$$

where σ_y is the yield strength of the ECAPed Cu-Mg alloy, σ_{LF} is the lattice friction or the Peierls–Nabarro stress, σ_{SS} is the strength contribution from the solid solution strengthening, σ_D is the strength contribution from the dislocation strengthening and σ_{GB} is the strength contribution from the grain boundary strengthening. A previous research showed that σ_{LF} and σ_{SS} of the ECAPed Cu-Mg alloy had little relation with the number of ECAP passes, with the values of 68.3 and 48.7 MPa, respectively [15].

The strength contribution from the dislocation strengthening can be expressed as Equations (2) and (3) using a modified Taylor model [39–41]:

$$\sigma_D = \alpha G M b \sqrt{\rho} \quad (2)$$

$$\rho = \frac{3(1-f)}{bL} \bar{\theta}_{LABs} \quad (3)$$

where α is a constant taken as 0.24 [42], G is the shear modulus taken as 45.6 GPa [42], M is the Taylor factor taken as 3.06 [42], b is the Burger's vector taken as 0.256 nm [42], ρ is the dislocation density, f is the fraction of HABs, $\bar{\theta}_{LABs}$ is the mean misorientation angle of LABs and L is the mean boundary spacing. It should be noted that this work assumes all dislocations to be the LABs with the misorientation angles lower than 15° but larger than 2°. Thus, it neglects the LABs with misorientation angles less than 2° and the individual dislocations between LABs. There are two reasons. One is that the EBSD examination is related to the angular resolution besides the lateral and longitudinal resolutions. The angular resolution usually is about 1° when no particular care is imposed on the EBSD examination [43]. Thus, a safe and popular operation is to take 2° as the lower limit of the misorientation angle of LABs. The other is that the ECAP process is one of severe plastic deformation and the evolution of dislocation configurations is faster than that of the conventional

deformation method. For example, the mean misorientation angles of LABs in the central and bottom regions were more than 4° after only one ECAP pass. This indicates that a number of dislocations were stored in the distinguishable LABs whose misorientation angles were much more than 2° . In other words, the dislocations stored in the LABs with misorientation angles less than 2° and the individual dislocations between LABs were subordinate and negligible.

The strength contribution from the grain boundary strengthening can be expressed as Equation (4) using a modified Hall–Petch relationship [39–41]:

$$\sigma_{GB} = k\sqrt{f/d} \quad (4)$$

where k is a material parameter taken as $0.14 \text{ MPa}\cdot\text{m}^{-1/2}$ [42], and d is the average grain size. It should be noted that there is an apparent difference between the modified and conventional Hall–Petch relationships, that is, the fraction of HABs (f) is introduced as the modified factor. It can be understood in this way. The ECAP process caused the well-developed dislocation structures where a number of LABs exist in the grains divided by HABs. Qualitatively, when dislocations attempt to slide in the grains and pile-up in the front of the grain boundaries, the LABs have impeded the motion of these dislocations. The strengthening mechanism in this case is different from that in the conventional case where the dislocations slide casually and only grain boundaries impede their motion. Thus, it needs a parameter to decrease the ability of the conventional grain boundary strengthening. Quantitatively, the grain radius ($d/2$) is inversely proportional to the grain boundary area per unit volume [40]. Thus, for the grain containing a number of LABs, it also needs to use the fraction of HABs to modify the grain boundary area per unit volume.

Figure 7 shows the calculated and experimental yield strengths in the central and bottom regions of the ECAPed Cu-Mg alloy, and Table 1 additionally shows their strength contributions from the various strengthening mechanisms. For the central region, the experimental yield strengths have been reported in the literature [15]. For the bottom region, it is impossible to perform a standard tensile testing due to the dimensional limit of the ECAPed billets, and thus only the calculated yield strengths are listed. Before the ECAP process, the Cu-Mg alloy shows a much lower experimental yield strength of only 124 MPa due to the dynamic recrystallized microstructure [15]. After one ECAP pass, the experimental yield strength increases significantly to 370 MPa. The calculated yield strength in the central region (344.7 MPa) shows that the improvement should be mainly attributed to the strength contribution from the dislocation strengthening (205.9 MPa) and the grain boundary strengthening (21.8 MPa). In addition, the calculated yield strength in the bottom region (291.4 MPa) is 53.3 MPa lower than that in the central region, showing a 16% difference where 46.6 MPa is from the dislocation strengthening and 6.7 MPa is from the grain boundary strengthening. Such a great strength difference is apparently resulted from the microstructure difference in the two regions. With the number of ECAP passes, the constantly accumulated dislocations are absorbed by the subgrain boundaries, leading to the increase in the misorientation angle and the formation of the HABs. Thus, the strength contributions from the dislocation strengthening and grain boundary strengthening enhance, resulting in continuous improvements in the yield strengths. Finally, after eight ECAP passes, the experimental yield strength achieves a high value of 548 MPa. The calculated yield strength in the central region (555.0 MPa) shows that the strength contributions from the dislocation strengthening (335.8 MPa) and grain boundary strengthening (102.2 MPa) are predominant, accounting for 78.9% in the whole. In addition, with the number of ECAP passes, the strength difference in the two regions gradually weakens and nearly disappears. For example, the difference decreases from 16% after one ECAP pass to 10% after two ECAP passes, and further decreases to 2%–4% in the subsequent ECAP process.

An important point is that the effect of the dislocation strengthening is much more significant than the effect of the grain boundary strengthening according to the above-mentioned calculated result. This is different from the conventional view that the UFGed materials are mainly strengthened by the grain boundary strengthening. This question should depend on how to define the dislocation strengthening and the grain boundary strengthening. In this work, the grain boundaries are considered as HABs with misorientation angles larger than 15° and the dislocations are considered to be stored in LABs with the misorientation angles lower than 15° but larger than 2° . Some

researchers hold the view that the boundaries with misorientation angles larger than 5° or 10° play a similar role in strengthening, just like the grain boundaries providing grain boundary strengthening. Thus, these boundaries are also generalized as grain boundaries. It results in the difference in considering the dislocation strengthening and the grain boundary strengthening for different research works. In addition, characterization methods also significantly affect how to distinguish the grain boundaries (or called HABs) and subgrain boundaries (or called LABs). For the EBSD examination, the misorientation angles of material elements are original data. How to define boundaries is dependent on researchers. For the TEM examination, however, the grain boundaries are mainly distinguished according to the contrast of the bright-field image. For example, Figures 4 and 5 in the reference [23] show some bright-field images of ECAPed pure Al and Al alloy, respectively. These so-called grains are adjacent to each other but show similar contrast. Apparently, the similar contrast means the similar orientations of these grains. Then, these grains actually are subgrains divided by LABs rather than grains divided by HABs. This also results in the overestimation of the grain boundary strengthening and the underestimation of the dislocation strengthening.

Figure 8 shows the relationship between the calculated yield strength and the measured hardness in the central and bottom regions of the ECAPed Cu-Mg alloy. However, the result is unclear. For the first six ECAP passes, the calculated yield strength and the measured hardness show a good linear relationship and high correlation coefficients more than 0.99. However, after eight ECAP passes, the correlation coefficients between the calculated yield strength and the measured hardness decrease to 0.96–0.97. From the variation trends of them, the increment of the calculated yield strength per the increment of the measured hardness increases sharply after eight ECAP passes. Thus, the linear relationship between the calculated yield strength and the measured hardness is predicted to be worse for more than eight ECAP passes.

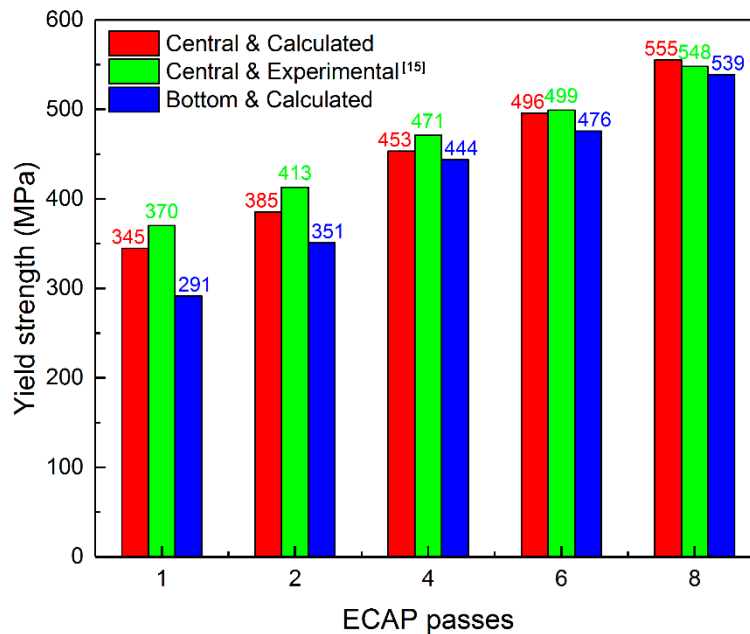


Figure 7. Calculated and experimental ^[15] yield strengths in the central and bottom regions of the ECAPed Cu-Mg alloy.

Table 1. The strength contributions from various strengthening mechanisms and the calculated and experimental yield strengths.

Region	ECAP Passes	σ_{LF} (MPa)	σ_{SS} (MPa)	σ_D (MPa)	σ_{GB} (MPa)	σ_y^{cal} (MPa)	σ_y^{exp} (MPa)
Central	1	68.3	48.7	205.9	21.8	344.7	370 ^[15]
	2	68.3	48.7	237.7	30.8	385.4	413 ^[15]
	4	68.3	48.7	280.8	55.5	453.3	471 ^[15]
	6	68.3	48.7	294.3	84.5	495.8	499 ^[15]
	8	68.3	48.7	335.8	102.2	555.0	548 ^[15]
Bottom	1	68.3	48.7	159.3	15.1	291.4	
	2	68.3	48.7	209.1	24.6	350.8	
	4	68.3	48.7	279.0	47.9	443.9	
	6	68.3	48.7	286.7	72.7	475.8	
	8	68.3	48.7	332.8	89.0	538.8	

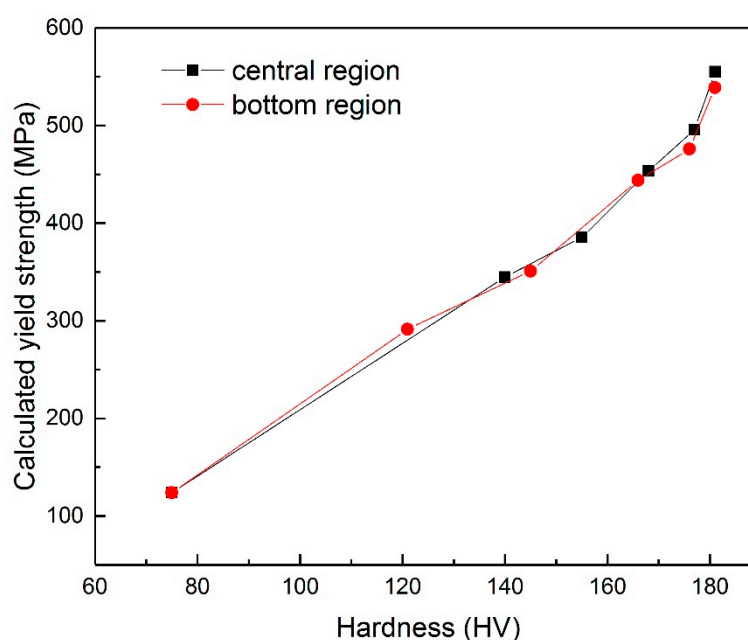


Figure 8. Relationship between the calculated yield strength and the measured hardness in the central and bottom regions of the ECAPed Cu-Mg alloy.

5. Conclusions

1. The hardness of a Cu-0.43Mg (wt.%) alloy was improved significantly at the initial stage of ECAP process, and the lower-hardness region appeared at the area nearby the bottom surface. With the number of ECAP passes, the hardness gently increased and finally became saturated. The inhomogeneity of the hardness distribution along the normal direction gradually weakened and finally disappeared;
2. The shear microstructure in the central region was different from that in the bottom region after one ECAP pass, and they became similar to each other after two ECAP passes, except the rotation angle of the elongated grains. With the further increasing ECAP passes, there was no obvious microstructure difference between the central and bottom regions;
3. The inhomogeneities of the hardness and the microstructure along the normal direction should be attributed to the non-zero outer arc of curvature of the ECAP die and the friction between the bottom surface of the billets and the ECAP die walls;
4. The strengthening mechanisms showed that the improvement of yield strengths should be mainly attributed to the strength contribution from the dislocation strengthening and the grain

boundary strengthening. For example, after eight ECAP passes, they accounted for 78.9% of the yield strength of 555.0 MPa.

Author Contributions: Formal analysis, M.M and X.Z.; Funding acquisition, Z.L., Z.X. (Zhu Xiao) and Hongyun Jiang; Investigation, M.M., X.Z., H.H. and Z.X. (Zhu Xiao); Methodology, M.M.; Project administration, Z.L., Z.X. (Ziqi Xia) and H.J.; Resources, Z.L. and Z.X. (Zhu Xiao); Supervision, Z.L., Z.X. (Zhu Xiao) and H.J.; Validation, M.M. and X.Z.; Writing—original draft, M.M.; Writing—review and editing, Z.X. (Zhu Xiao). All authors have read and agreed to the published version of the manuscript.

Funding: This research was funded by the National Key Research and Development Program of China (Grant No. 2016YFB0301300), National Natural Science Foundation of China (Grant No. 51974375), Technology Research Program of Ningbo, China (Grant No. 2019B10088), and Project of State Key Laboratory of Powder Metallurgy, Central South University, Changsha, China.

Acknowledgments: Thanks are also given to Dr. Zhilei Zhao for his help.

Conflicts of Interest: The authors declare no conflict of interest.

References

1. Feng, J.; Liang, S.; Guo, X.; Zhang, Y.; Song, K. Electrical conductivity anisotropy of copper matrix composites reinforced with SiC whiskers. *Nanotechnol. Rev.* **2019**, *8*, 285–292, doi:10.1515/ntrev-2019-0027.
2. Zhao, Z.; Xiao, Z.; Li, Z.; Qiu, W.; Jiang, H.; Lei, Q.; Liu, Z.; Jiang, Y.; Zhang, S. Microstructure and properties of a Cu–Ni–Si–Co–Cr alloy with high strength and high conductivity. *Mater. Sci. Eng. A* **2019**, *759*, 396–403, doi:10.1016/j.msea.2019.05.003.
3. Li, S.; Guo, X.; Zhang, S.; Feng, J.; Song, K.; Liang, S. Arc erosion behavior of TiB₂/Cu composites with single-scale and dual-scale TiB₂ particles. *Nanotechnol. Rev.* **2019**, *8*, 619–627.
4. Feng, J.; Song, K.; Liang, S.; Guo, X.; Jiang, Y. Electrical wear of TiB₂ particle-reinforced Cu and Cu–Cr composites prepared by vacuum arc melting. *Vacuum* **2020**, *175*, 109295, doi:10.1016/j.vacuum.2020.109295.
5. Ji, G.; Li, Q.; Li, L. The kinetics of dynamic recrystallization of Cu–0.4Mg alloy. *Mater. Sci. Eng. A* **2013**, *586*, 197–203, doi:10.1016/j.msea.2013.07.083.
6. Ji, G.; Yang, G.; Li, L.; Li, Q. Modeling Constitutive Relationship of Cu-0.4 Mg Alloy During Hot Deformation. *J. Mater. Eng. Perform.* **2014**, *23*, 1770–1779, doi:10.1007/s11665-014-0912-0.
7. Yuan, Y.; Dai, C.; Li, Z.; Yang, G.; Liu, Y.; Xiao, Z. Microstructure evolution of Cu–0.2Mg alloy during continuous extrusion process. *J. Mater. Res.* **2015**, *30*, 2783–2791, doi:10.1557/jmr.2015.237.
8. Yuan, Y.; Li, Z.; Xiao, Z.; Zhao, Z. Investigations on Voids Formation in Cu–Mg Alloy During Continuous Extrusion. *JOM* **2017**, *69*, 1696–1700, doi:10.1007/s11837-017-2469-5.
9. Zhen, G.; Kim, Y.; Haochuang, L.; Koo, J.-M.; Seok, C.-S.; Lee, K.; Kwon, S.-Y. Bending fatigue life evaluation of Cu–Mg alloy contact wire. *Int. J. Precis. Eng. Manuf.* **2014**, *15*, 1331–1335, doi:10.1007/s12541-014-0473-z.
10. Zhang, X.; Han, J.; Chen, L.; Zhou, B.; Xue, Y.; Jia, F. Effects of B and Y additions on the microstructure and properties of Cu–Mg–Te alloys. *J. Mater. Res.* **2013**, *28*, 2747–2752, doi:10.1557/jmr.2013.266.
11. Duan, Y.; Xu, G.; Tang, L.; Li, Z.; Yang, G. Microstructure and properties of the novel Cu–0.30Mg–0.05Ce alloy processed by equal channel angular pressing. *Mater. Sci. Eng. A* **2015**, *648*, 252–259, doi:10.1016/j.msea.2015.09.078.
12. Ha, S.-H.; Yoon, Y.-O.; Lim, H.-K.; Kim, S.K. Effect of Heat Treatment on Microstructure and Hardness of Cu–Mg Alloy with a Trace of Ca. *J. Nanosci. Nanotechnol.* **2017**, *17*, 7820–7823, doi:10.1166/jnn.2017.14845.
13. Li, Y.; Xiao, Z.; Li, Z.; Zhou, Z.; Yang, Z.; Lei, Q. Microstructure and properties of a novel Cu–Mg–Ca alloy with high strength and high electrical conductivity. *J. Alloy. Compd.* **2017**, *723*, 1162–1170, doi:10.1016/j.jallcom.2017.06.155.
14. Freudenberger, J.; Kauffmann, A.; Klauß, H.; Marr, T.; Nenkov, K.; Sarma, V.; Schultz, L. Studies on recrystallization of single-phase copper alloys by resistance measurements. *Acta Mater.* **2010**, *58*, 2324–2329, doi:10.1016/j.actamat.2009.12.018.
15. Ma, M.; Li, Z.; Qiu, W.; Xiao, Z.; Zhao, Z.; Jiang, Y. Microstructure and properties of Cu–Mg–Ca alloy processed by equal channel angular pressing. *J. Alloy. Compd.* **2019**, *788*, 50–60, doi:10.1016/j.jallcom.2019.01.335.
16. Valiev, R.Z.; Langdon, T.G. Principles of equal-channel angular pressing as a processing tool for grain refinement. *Prog. Mater. Sci.* **2006**, *51*, 881–981, doi:10.1016/j.pmatsci.2006.02.003.

17. Cobos, O.F.H.; Berrios-Ortiz, J.A.; Cabrera, J.M. Texture and fatigue behavior of ultrafine grained copper produced by ECAP. *Mater. Sci. Eng. A* **2014**, *609*, 273–282, doi:10.1016/j.msea.2014.05.011.
18. Wei, W.; Wang, S.L.; Wei, K.X.; Alexandrov, I.V.; Du, Q.B.; Hu, J. Microstructure and tensile properties of Cu Al alloys processed by ECAP and rolling at cryogenic temperature. *J. Alloy. Compd.* **2016**, *678*, 506–510, doi:10.1016/j.jallcom.2016.04.035.
19. Zaynullina, L.; Alexandrov, I.V.; Wei, W. Effect of the stacking fault energy on the mechanical properties of pure Cu and Cu-Al alloys subjected to severe plastic deformation. *MATEC Web Conf.* **2017**, *129*, 2032, doi:10.1051/mateconf/201712902032.
20. Wongsan-Ngam, J.; Wen, H.; Langdon, T.G. Microstructural evolution in a Cu–Zr alloy processed by a combination of ECAP and HPT. *Mater. Sci. Eng. A* **2013**, *579*, 126–135, doi:10.1016/j.msea.2013.05.010.
21. Mishnev, R.; Shakhova, I.; Belyakov, A.; Kaibyshev, R. Deformation microstructures, strengthening mechanisms, and electrical conductivity in a Cu–Cr–Zr alloy. *Mater. Sci. Eng. A* **2015**, *629*, 29–40, doi:10.1016/j.msea.2015.01.065.
22. Iwahashi, Y.; Wang, J.; Horita, Z.; Nemoto, M.; Langdon, T.G. Principle of equal-channel angular pressing for the processing of ultra-fine grained materials. *Scr. Mater.* **1996**, *35*, 143–146, doi:10.1016/1359-6462(96)00107-8.
23. Xu, C.; Furukawa, M.; Horita, Z.; Langdon, T.G. The evolution of homogeneity and grain refinement during equal-channel angular pressing: A model for grain refinement in ECAP. *Mater. Sci. Eng. A* **2005**, *398*, 66–76, doi:10.1016/j.msea.2005.03.083.
24. Xu, C.; Langdon, T.G. The development of hardness homogeneity in aluminum and an aluminum alloy processed by ECAP. *J. Mater. Sci.* **2007**, *42*, 1542–1550, doi:10.1007/s10853-006-0899-5.
25. Beyerlein, I.; Toth, L.S. Texture evolution in equal-channel angular extrusion. *Prog. Mater. Sci.* **2009**, *54*, 427–510, doi:10.1016/j.pmatsci.2009.01.001.
26. Prell, M.; Xu, C.; Langdon, T.G. The evolution of homogeneity on longitudinal sections during processing by ECAP. *Mater. Sci. Eng. A* **2008**, *480*, 449–455, doi:10.1016/j.msea.2007.08.011.
27. Alhajeri, S.N.; Gao, N.; Langdon, T.G. Hardness homogeneity on longitudinal and transverse sections of an aluminum alloy processed by ECAP. *Mater. Sci. Eng. A* **2011**, *528*, 3833–3840, doi:10.1016/j.msea.2011.01.074.
28. Reihanian, M.; Ebrahimi, R.; Moshksar, M.; Terada, D.; Tsuji, N. Microstructure quantification and correlation with flow stress of ultrafine grained commercially pure Al fabricated by equal channel angular pressing (ECAP). *Mater. Charact.* **2008**, *59*, 1312–1323, doi:10.1016/j.matchar.2007.11.006.
29. Ma, M.; Li, Z.; Qiu, W.; Xiao, Z.; Zhao, Z.; Jiang, Y.; Xia, Z.; Huang, H. Development of homogeneity in a Cu-Mg-Ca alloy processed by equal channel angular pressing. *J. Alloy. Compd.* **2020**, *820*, 153112, doi:10.1016/j.jallcom.2019.153112.
30. Kim, H.S. Evaluation of Strain Rate During Equal-channel Angular Pressing. *J. Mater. Res.* **2002**, *17*, 172–179, doi:10.1557/jmr.2002.0026.
31. Kim, H.S. Finite element analysis of deformation behaviour of metals during equal channel multi-angular pressing. *Mater. Sci. Eng. A* **2002**, *328*, 317–323, doi:10.1016/s0921-5093(01)01793-2.
32. Kim, H.S.; Seo, M.H.; Hong, S.I. Finite element analysis of equal channel angular pressing of strain rate sensitive metals. *J. Mater. Process. Technol.* **2002**, *130*, 497–503, doi:10.1016/s0924-0136(02)00796-3.
33. Beyerlein, I.; Tomé, C. Analytical modeling of material flow in equal channel angular extrusion (ECAE). *Mater. Sci. Eng. A* **2004**, *380*, 171–190, doi:10.1016/j.msea.2004.03.063.
34. Suh, J.-Y.; Kim, H.-S.; Park, J.-W.; Chang, J.-Y. Finite element analysis of material flow in equal channel angular pressing. *Scr. Mater.* **2001**, *44*, 677–681, doi:10.1016/s1359-6462(00)00645-x.
35. Deng, G.; Lu, C.; Su, L.; Liu, X.; Tieu, A. Modeling texture evolution during ECAP of copper single crystal by crystal plasticity FEM. *Mater. Sci. Eng. A* **2012**, *534*, 68–74, doi:10.1016/j.msea.2011.11.042.
36. Skrotzki, W.; Toth, L.S.; Klöden, B.; Brokmeier, H.-G.; Arruffat-Massion, R. Texture after ECAP of a cube-oriented Ni single crystal. *Acta Mater.* **2008**, *56*, 3439–3449, doi:10.1016/j.actamat.2008.03.017.
37. Yang, G.; Li, Z.; Yuan, Y.; Lei, Q. Microstructure, mechanical properties and electrical conductivity of Cu–0.3Mg–0.05Ce alloy processed by equal channel angular pressing and subsequent annealing. *J. Alloy. Compd.* **2015**, *640*, 347–354, doi:10.1016/j.jallcom.2015.03.218.
38. Lei, Q.; Li, Z.; Gao, Y.; Peng, X.; Derby, B. Microstructure and mechanical properties of a high strength Cu-Ni-Si alloy treated by combined aging processes. *J. Alloy. Compd.* **2017**, *695*, 2413–2423, doi:10.1016/j.jallcom.2016.11.137.

39. Luo, P.; McDonald, D.; Xu, W.; Palanisamy, S.; Dargusch, M.; Xia, K. A modified Hall–Petch relationship in ultrafine-grained titanium recycled from chips by equal channel angular pressing. *Scr. Mater.* **2012**, *66*, 785–788, doi:10.1016/j.scriptamat.2012.02.008.
40. Hansen, N. Hall–Petch relation and boundary strengthening. *Scr. Mater.* **2004**, *51*, 801–806, doi:10.1016/j.scriptamat.2004.06.002.
41. Hansen, N. Boundary strengthening in undeformed and deformed polycrystals. *Mater. Sci. Eng. A* **2005**, *409*, 39–45, doi:10.1016/j.msea.2005.04.061.
42. Rodriguez-Calvillo, P.; Ferrer, N.; Cabrera, J.M. Analysis of microstructure and strengthening in CuMg alloys deformed by equal channel angular pressing. *J. Alloy. Compd.* **2015**, *626*, 340–348, doi:10.1016/j.jallcom.2014.12.043.
43. Germain, L.; Kratsch, D.; Salib, M.; Gey, N. Identification of sub-grains and low angle boundaries beyond the angular resolution of EBSD maps. *Mater. Charact.* **2014**, *98*, 66–72, doi:10.1016/j.matchar.2014.10.007.



© 2020 by the authors. Licensee MDPI, Basel, Switzerland. This article is an open access article distributed under the terms and conditions of the Creative Commons Attribution (CC BY) license (<http://creativecommons.org/licenses/by/4.0/>).